Geo-Energy Research

Original article

Mechanisms of feldspar dissolution and associated authigenic mineral precipitation in coal measure tight sandstone reservoirs: Insights using a reaction-transport numerical model incorporating organic chelation

Weikai Huang¹, Kelai Xi¹⁰*, Yingchang Cao¹, Xiang Shan², Zhicheng Cui¹, Helge Hellevang³

Keywords:

Coal-measure tight sandstone feldspar dissolution authigenic mineral precipitation organic chelation mass transfer reaction-transport model

Cited as:

Huang, W., Xi, K., Cao, Y., Shan, X., Cui, Z., Hellevang, H. Mechanisms of feldspar dissolution and associated authigenic mineral precipitation in coal measure tight sandstone reservoirs: Insights using a reaction-transport numerical model incorporating organic chelation. Advances in Geo-Energy Research, 2025, 18(1): 51-68. https://doi.org/10.46690/ager.2025.10.05

Abstract:

Feldspar dissolution plays a pivotal role in the development of reservoirs. However, our knowledge of the controlling mechanisms of organic chelation and the effect of other factors on feldspar dissolution and authigenic mineral precipitation in coal-measure reservoirs remain insufficient. This study investigates the dissolution-precipitation mechanisms and their impacts on secondary porosity development through integrated petrological, geochemical and numerical simulation. Petrographic analysis reveals a distinctive spatial decoupling of feldspar dissolution and authigenic mineral precipitation: Sandstones adjacent to coal seams exhibit enhanced feldspar dissolution but limited kaolinite precipitation, whereas kaolinite peaks anomalously in mid-lithofacies zones. Through numerical simulations, significant solute migration is revealed under the constraints of organic chelation at 65 and 100 °C, and the principal stage of effective secondary porosity development is identified as early diagenetic stage B to middle diagenetic stage A1. Organic acid, temperature and flow rate are the key controlling factors on feldspar dissolution and authigenic mineral precipitation. Oxalic acid enhances feldspar dissolution via aqueous chelation and a reinforced proton-promoting mechanism, and the resultant Al-oxalate chelates suppress kaolinite precipitation. The feldspar dissolution rates increase exponentially with temperature elevation, driving subsequent authigenic mineral precipitation. Meanwhile, the flow rate controls solute transport efficiency. Rapid flow in low-temperature open systems facilitates long-distance solute export and inhibits mineral precipitation, whereas stagnant flow in high-temperature closed systems constrains feldspar dissolution and enhances authigenic precipitation. Given the global prevalence of coal-measure reservoirs, the proposed dissolution-precipitation model provides critical insights for the evolution of secondary porosity in coal-measure sandstone reservoirs.

1. Introduction

In deep tight sandstone reservoirs, feldspar dissolution by organic acids constitutes a fundamental mechanism of secondary porosity generation and high-quality reservoir development (Bennett and Siegel, 1987; Yuan et al., 2013; Liu et al., 2018; Xi et al., 2024). However, organic acids generated from coal-measure source rocks differ significantly from those

Yandy Scientific Press *Corresponding author.

E-mail address: m15060578935@163.com (W. Huang); xikelai@upc.edu.cn (K. Xi); caoych@upc.edu.cn (Y. Cao); shanx_hz@petrochina.com.cn (X. Shan); Czc@s.upc.edu.cn (Z. Cui); helge.hellevang@geo.uio.no (H. Hellevang). 2207-9963 © The Author(s) 2025.

Received July 21, 2025; revised August 20, 2025; accepted September 15, 2025; available online September 19, 2025.

¹State Key Laboratory of Deep Oil and Gas, China University of Petroleum (East China), Qingdao 266580, P. R. China

²PetroChina Hangzhou Institute of Petroleum Geology, Hangzhou 310023, P. R. China

³Department of Geosciences, University of Oslo, Oslo 0316, Norway

derived from lacustrine mudstones/shales, potentially resulting in distinct distribution patterns of feldspar dissolution and authigenic mineral precipitation (Li et al., 2021). Therefore, elucidating the mechanisms of how coal-derived organic acids influence feldspar dissolution and authigenic mineral precipitation is of great significance for understanding the evolution of secondary porosity in coal-bearing reservoirs. Laboratory experiments have confirmed the dissolution capacity of organic acids (Manley and Evans, 1986; Welch and Ullman, 1996), yet the types and amounts of organic acids varies substantially depending on kerogen type and thermal maturity. Coal began to produce organic acid during the early shallow diagenetic stage (equivalent to stage B from Cao et al. (2022), this stage corresponds to a temperature interval of 50 to 80 °C), whose amount can reach 6 times that in lacustrine mudstone (Li et al., 2021). Type III kerogen in coal generates not only monocarboxylic acids but also abundant dicarboxylic acids, particularly oxalic acid (Kawamura and Kaplan, 1987; Zhu et al., 2019). Previous studies revealed the superior dissolution efficacy of oxalic acid, attributed to its high H⁺ donation capacity and organic chelation (Surdam et al., 1984; Lin et al., 2023). In fact, the organic chelation of oxalic acid to promote feldspar has been widely demonstrated. This chelation mechanism reduces Al3+ concentrations in pore fluids and significantly increases the apparent solubility of feldspar (Welch and Ullman, 1993; Dong et al., 2019). To summarize, feldspars in coal-measure tight sandstone are more susceptible to dissolution, leading to the formation of secondary porosity reservoirs (Bevan and Savage, 1989; Zhu et al., 2015; Liu et al., 2018; Li et al., 2019; Shan et al., 2021).

The formation of secondary porosity by feldspar dissolution is a complex mechanism involving factors such as temperature, diagenetic fluids, feldspar type, and the diagenetic system. The critical controlling factors of dissolution efficacy include temperature conditions, availability of diagenetic fluids, and feldspar type (Sorai et al., 2005; Kampman et al., 2009; Hellevang et al., 2013; Yang et al., 2014). The degree of openness of the diagenetic system (formation water flow rate) constrains the transfer of solutes and is a crucial factor determining whether feldspar dissolution can effectively increase porosity (Steefel and Maher, 2009; Gao et al., 2017; Yuan et al., 2017). The elemental mobility differentials during mass transfer are particularly pronounced. In closed diagenetic systems, monovalent cations (K+, Na+, Ca2+) demonstrate high transport capacity, whereas trivalent Al3+ and tetravalent Si⁴⁺ exhibit restricted mobility (Giles and De Boer, 1990). During the middle diagenetic stage A1 (80-110 °C; Cao et al., 2022), reservoir burial depths exceeding several kilometers correspond to a formation water flow rate < 0.01 m/yr, restricting Al³⁺ and SiO₂(aq) transport to diffusion-dominated processes at centimeter-to-meter scales in unfractured reservoirs (Giles, 1987; Ma et al., 2017). However, during the process of organic acid-mediated organic-inorganic interactions in deeply buried reservoirs, the chelation of aqueous Al by carboxylate ions may significantly alter the precipitation distribution of kaolinite (Lawrence et al., 2014). For instance, Blake and Walter (1996) conducted simulated feldspar dissolution experiments containing 3 mmol oxalic acid and 0.5 mmol citric acid and observed that the precipitation of secondary minerals (kaolinite) was markedly inhibited, confirming the role of organic acids in suppressing kaolinite precipitation. Consequently, in coal-bearing diagenetic systems, the presence and reactions of organic acids may significantly impact the development of secondary porosity within reservoirs.

While laboratory experiments have established the fundamental role of organic acids in feldspar dissolution, they often overlooked the spatial effects of organic acids in enhancing dissolution and promoting mass transfer during different diagenetic stages (Barclay and Worden, 2000; Yuan et al., 2017; Li et al., 2024). Therefore, elucidating the mechanisms of coalderived organic acid-driven feldspar dissolution and associated authigenic precipitation across the diagenetic stages is crucial for understanding the diagenetic evolution and secondary porosity of coal-bearing reservoirs. This study aims to elucidate these mechanisms by integrating petrographic analysis with PHREEQC-based geochemical simulations of the Jurassic Badaowan Formation reservoirs. Our work specifically focuses on (1) delineating the spatial distribution patterns of feldspar dissolution and authigenic minerals across different lithofacies, and (2) unraveling their genetic relationships under the influence of coal-derived organic acids through PHREEQC-based geochemical simulations.

2. Methodology

2.1 Geological background

The Junggar Basin is a major petroliferous basin in Western China, with an area of about 13.5×10^4 km². It can be divided into six first-order structural units and further subdivided into 44 second-order structural units (Fig. 1(a)) (Zhang et al., 2022). The study area is situated within the Mobei Uplift and the Mosowan Uplift in the central depression of the Junggar Basin (Figs. 1(a) and 1(b)). It borders the Donghaidaozi Sag to the east, the Monan Uplift, the Shawan Sag, and the Fukang Sag to the south, the Penyijingxi Sag to the west, and the Dinan Uplift to the north (Gao et al., 2017). The Jurassic System in the central Junggar Basin comprises terrigenous clastic deposits predominantly characterized by alluvial fan-fluvial-deltaic-lacustrine depositional systems. In stratigraphical terms, the sequence is subdivided into the Lower Jurassic Badaowan and Sangonghe Formations, overlain by the Middle Jurassic Xishanyao and Toutunhe Formations (Fig. 1(c)). The Upper Jurassic Qigu and Kalazha Formations, however, are absent from the study area due to the extensive denudation associated with the Yanshanian tectonic activity (Lin et al., 2022). The Badaowan Formation (J₁b) is stratigraphically partitioned into three members $(J_1b^1, J_1b^2,$ J_1b^3) from bottom to top. This period witnessed basin-wide stable subsidence accompanied by extensive terrestrial clastic accumulation. The J_1b^1 member is marked by the extensive occurrence of braided-river delta facies glutenite deposits. In the J_1b^2 deposition stage, influenced by a transgressive event, a large suite of stable and thick lacustrine mudstones was deposited. As the lake regressed during the deposition of the J₁b³ member, braided-river delta facies deposits were formed once again (Sun et al., 2017). The warm-humid Early

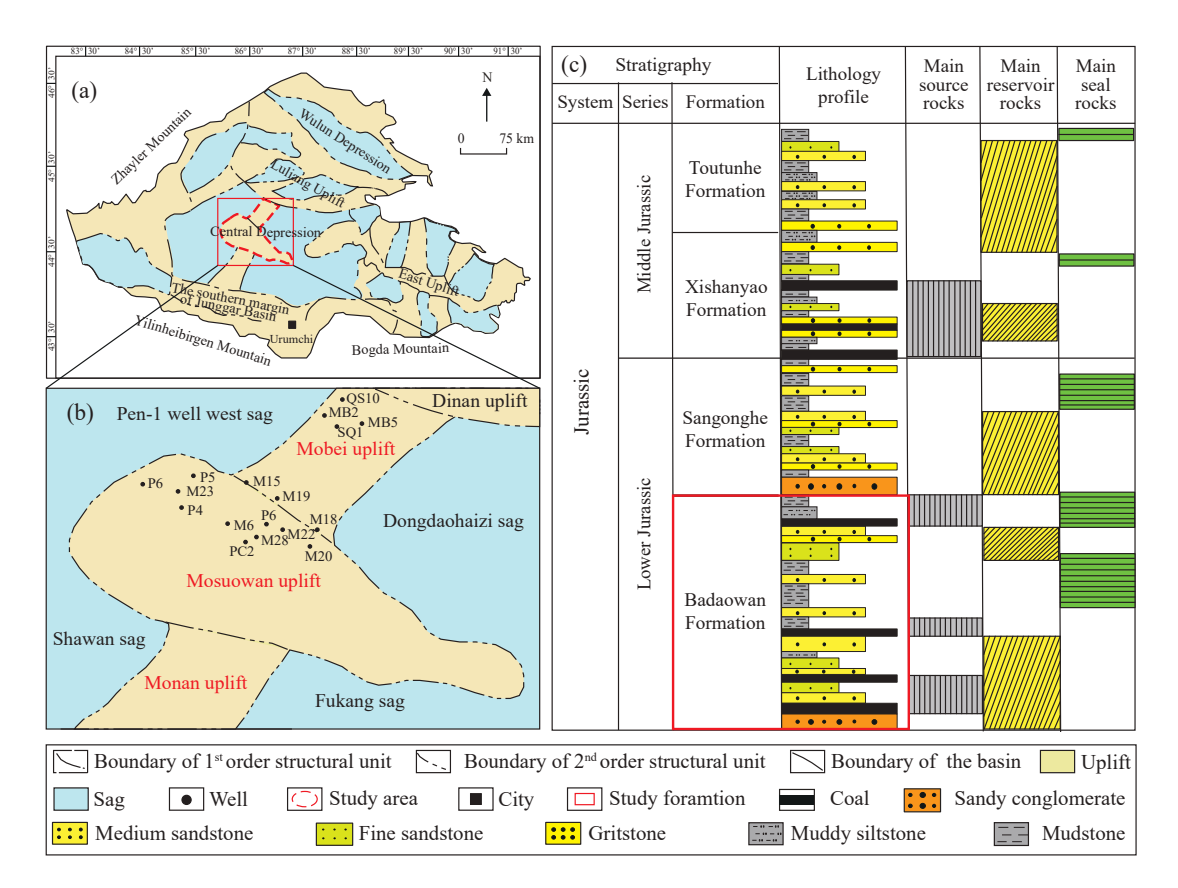


Fig. 1. (a)-(b) Regional tectonic location of the Junggar Basin and (c) the stratigraphic developmental characteristics of the Badaowan Formation.

Jurassic paleoclimate supported prolific vegetation, driving coal seam formation in both J_1b^1 and J_1b^3 members (Meng et al., 2023; Yu et al., 2023). These carbonaceous horizons serve as regional stratigraphic markers for lithological correlation (He et al., 2004).

2.2 Sample and experimental method

This study systematically investigated 76 sandstone samples from the Badaowan formation. Seventy-two blue-epoxyimpregnated thin sections were analyzed via polarized light microscopy to determine the mineral composition, pore characteristics, and identify diagenetic phenomena. Detailed quartz overgrowth was detected through cathodoluminescence (CL) microscopy performed using a Zeiss Axioscope A1 APOL system equipped with CL8200MK detector (accelerating voltage: 10 kV, beam current: 250 µA). For quantitative petrographic analysis, a grid-based photomicrograph acquisition protocol was implemented: Medium-coarse grained sandstones were systematically imaged at 200 µm scale through 16 orientation-specific captures per thin section. These 16 images were then composited in CorelDRAW, where the secondary porosity and the authigenic minerals such as kaolinite and quartz overgrowths were drawn and identified. The mineral composition of the 27 sandstone samples was analyzed using X-ray diffraction (XRD). Twenty-two thin sections and core samples were subjected to microscopic observation using a field emission scanning electron microscope (FE-SEM) to analyze the morphological characteristics of dissolution pores and authigenic minerals. Next, elemental analysis of the minerals was conducted using an energy dispersive spectrometer. To determine the homogenization temperatures and salinities of fluid inclusions within quartz overgrowths, more than 20 samples were prepared as double-polished wafers with a thickness of approximately 0.05 mm. The fluid inclusions were observed using a digital polarized light microscope (Axio Scope.A1). The utilized cold and hot stage was model THMSG600, which is capable of measuring temperatures ranging from -196 to 600 °C.

2.3 Formulation of reactive-transport model and input constraints

2.3.1 Model formulation

PHREEQC version 3.7 was employed to simulate the kinetic reactions of minerals and vertical reactive transport. Given the vertically interbedded distribution of sandstone and coal seams in natural reservoirs, fluid-rock interactions between coal and sandstone were modeled as a one-dimensional diffusive transport system. A 5-meter vertical column discretized into 50 grid cells (0.1 m per cell) was constructed, with cells 1-5 simulating coal layers capable of acidic fluid generation and cells 46-50 representing sandstone lithology (Fig. 2(a)). To systematically evaluate the evolutionary processes of feldspar dissolution and authigenic mineral precipitation in coal-bearing strata, geological time-scale simulations

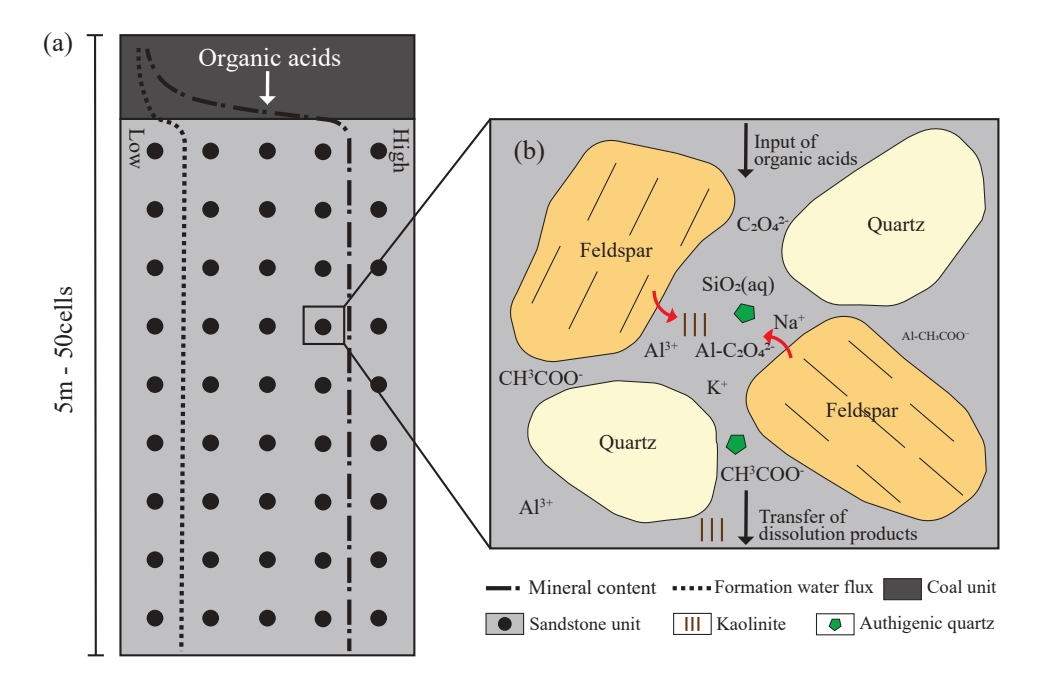


Fig. 2. (a) Coal-sandstone model description and (b) micro-scale fluid-rock interaction.

were conducted spanning 2,500 years under four distinct temperature regimes (25, 65, 100, 130 °C). These experimental conditions were designed to replicate the diagenetic environments of early diagenetic stage A (-50 °C), early diagenetic stage B (50-80 °C), middle diagenetic stage A1 (80-110 °C), and middle diagenetic stage A2 (110-150 °C). The flow rate of the formation water decreases exponentially from shallow burial to deep burial (Giles, 1987). According to the study by Cao et al. (2022), the diagenetic system transitions from open to closed conditions with increasing burial depth, corresponding to a temperature range from shallow burial (25-50 °C) to deep burial (150 °C). The associated flow rate ranges from approximately 10 to 0.001 m/yr; therefore, our model adopted this velocity range to reflect the system's evolution. The specific settings are shown in Table S1.

In order to account for the effects of early sediment compaction, this study considers the intimate contact between mineral grains and pore fluids, which significantly reduces reactive surface areas. Consequently, referring to the pore evolution of the sandstone in the Badaowan Formation (Ming et al., 2025), a water-rock mass ratio of 1:3 was adopted for each computational cell, corresponding to 750 g of minerals and 250 g of aqueous phase per kilogram of bulk material. Initial mineral assemblages were constrained through integrated petrographic thin-section analysis and XRD data: 25-100 °C simulations: Quartz (400 g, 6.66 mol), K-feldspar (100 g, 0.36 mol), albite (200 g, 0.76 mol), anorthite (50 g, 0.18 mol), with kaolinite initialized at 0 g; 130 °C simulation: Quartz (400 g, 6.66 mol), K-feldspar (100 g, 0.36 mol), albite (200 g, 0.72 mol), anorthite (30 g, 0.10 mol), kaolinite (10 g, 0.04 mol), with illite (10 g, 0.025 mol) represented using muscovite's thermodynamic parameters in PHREEQC.

2.3.2 Input of organic acids

The establishment of coal-derived organic acid simulation systems requires precise constraints on both organic acid generation and dissociation processes. In the Badaowan Formation coals, total organic carbon exhibits significant enrichment with values ranging from 65% to 90% (Shi et al., 2020). Accordingly, the total organic carbon parameter for coal cells in our simulation framework was standardized at 80%. The quantitative modeling of organic acid generation requires the rigorous incorporation of thermal evolution variations across diagenetic stages. The predicted organic acid yields in thermal reaction models were quantitatively constrained according to the temperature-dependent framework proposed by Andresen et al. (1994). Specifically, simulated outputs indicated maximum acid generation capacities of 0.1448 mol (25 °C), 0.2288 mol (65 °C), 0.8744 mol (100 °C), and 0.7696 mol (130 °C). Referring to the pyrolysis and hydrocarbon generation kinetics of coal, the kinetic rate constant for coal acid generation in our geochemical model was parameterized as $\log k = -12$ (Andresen et al., 1994; Li et al., 2021; Zeng et al., 2021).

For Type III kerogen pyrolysis products, our model incorporates both monocarboxylic and dicarboxylic acids (Fig. 2(b)), specifically selecting acetic acid (dominant component) and oxalic acid (key chelator) based on their documented prevalence in thermal alteration products (Kawamura and Kaplan, 1987). According to Surdam and MacGowan (1987) and Kawamura and Kaplan (1987), the oxalic acid concentration of the model at 25-100 and 130 °C accounted for 20% and 10% of the total organic acids, respectively. The dissociation behavior of oxalic acid and its chelation reactions were parameterized using established thermodynamic models (Morrey et al., 1985; Burgos-Cara et al., 2017; Li et al., 2024), with detailed reaction schemes provided in Table S2. Given the negligible mineral content characteristic of these coals,

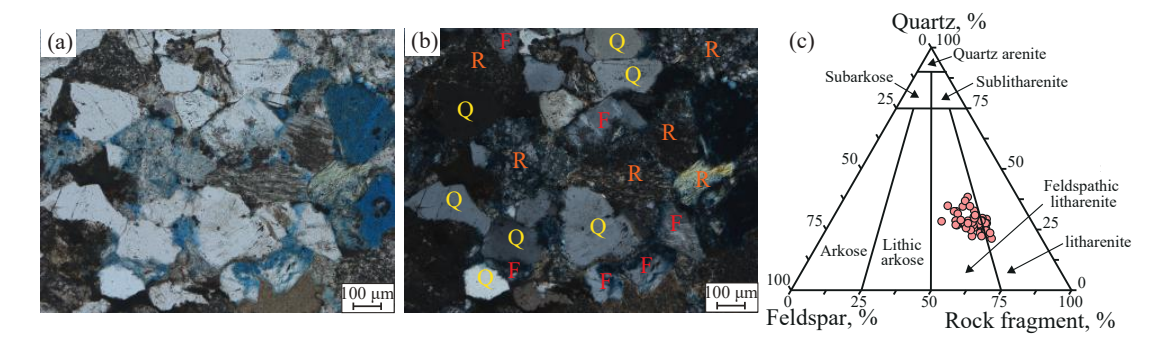


Fig. 3. Petrology characteristics of coal-measure reservoirs in the Badaowan Formation: (a)-(b) Textural and compositional features of the tight sandstones and (c) ternary map of clastic composition (classification of sandstone using Folk (1974)'s classification). Q-quartz, F-feldspar, R-rock fragment.

mineralogical components were excluded from the coal cell simulations.

2.3.3 Kinetic parameters of mineral diagenesis in simulation

In PHREEQC, the kinetic module allows for the definition of kinetic parameters related to mineral dissolution. During the simulations, a rate equation grounded in the Transition State Theory is utilized, as detailed below:

$$R_m = k_m S_m a_{H^+}^n \left(1 - \Omega \right) \tag{1}$$

where m represents the mineral index, R_m stands for the reaction rate, mol/s; k_m is the rate constant, mol/cm²/s; S_m denotes the specific surface area where the mineral reaction occurs, $a_{\rm H^+}$ is the activity of H⁺, n is the reaction order of H⁺ in the solution, and Ω represents the saturation ratio. The k_m values for many minerals are listed at 25 °C. The temperature dependence of km can be represented using the Van't Hoff equation given by:

$$k_m = k_{25} \exp\left[\frac{-E_a}{R} \left(\frac{1}{T} - \frac{1}{298.15}\right)\right]$$
 (2)

where E_a represents the apparent activation energy, kJ/mol; k_{25} denotes the reaction rate constant of the mineral at 25 °C, mol/cm²/s; R is the gas constant (8.314 J/[mol·K]), and T stands for the absolute temperature, K. The Table S3 provides a detailed list of the relevant kinetic parameters used in the kinetic module, with the k_{25} , E_a and n values for minerals such as potassium feldspar and quartz being sourced from the compilation by Palandri and Kharaka (2004).

Quantifying specific surface areas of natural rock minerals presents significant methodological challenges. Multiple analytical approaches exist for the determination of this parameter, including geometric surface area calculations and gas adsorption techniques (Harouiya and Oelkers, 2004). For feldspars and quartz, specific surface area values were adopted from the seminal work of Sonnenthal and Spyoher (2001). Similarly, kaolinite and muscovite surface area parameters were obtained from established datasets by Yang and Steefel (2008) and Köhler et al. (2003). In accordance with the experimental design requirements, the water-to-rock mass ratio was maintained at 1:3 throughout this study. This configuration implies

that only 25% of each mineral's total specific surface area remains accessible for chemical interactions due to geometric constraints. The comprehensive mineral-specific surface area data are systematically presented in Table S3.

2.3.4 Mass transport in simulation

Mass transport in natural porous media encompasses two mechanisms: Advection and dispersion, with dispersion being further divisible into mechanical dispersion and molecular diffusion. In PHREEQC, the conservation of mass principle, applied to a chemical undergoing transport, leads to the derivation of the advection-reaction-dispersion equation:

$$\frac{\partial C}{\partial t} = -v \frac{\partial C}{\partial x} + D_L \frac{\partial^2 C}{\partial x^2} - \frac{\partial q}{\partial t}$$
 where *C* represents the concentration in solution, mol/kgw; *t*

where C represents the concentration in solution, mol/kgw; t denotes time, s; v denotes the pore water rate, m/s; x denotes distance, m; D_L is the fluid dispersion coefficient, m²/s; with $D_L = D_e + \alpha_L v$, where D_e is the effective diffusion coefficient and α_L is the longitudinal dispersivity, m; and q denotes the concentration of a solid phase in the pore fluid, mol/kgw.

Mechanical dispersion is primarily defined through dispersivity. The transport model in PHREEQC is one-dimensional; therefore, only the longitudinal dispersivity needs to be considered. In actual geological formations, the molecular diffusion rates are closely related to temperature. According to Boudreau (1996), the difference in diffusion coefficients among K⁺, Al(OH)₃, Al³⁺, and SiO₂(aq) is small. To simplify the complexity of the model, the same effective diffusion coefficient is used in the initial setup, with values of 2.0×10^{-10} , 4.1×10^{-10} , 6.2×10^{-10} , and 8.3×10^{-10} cm²/s for the four simulated temperatures of 25, 65, 100, and 130 °C, respectively (Yuan et al., 2017).

3. Results

3.1 Petrographic feature

The tight sandstone of the Jurassic Badaowan Formation is mainly composed of quartz, feldspar and rock fragments (Figs. 3(a) and 3(b)). The particle size of sandstone clastic particles is mainly distributed between fine to coarse grains, the sorting is poor to medium, and the roundness is angular to sub-circular.

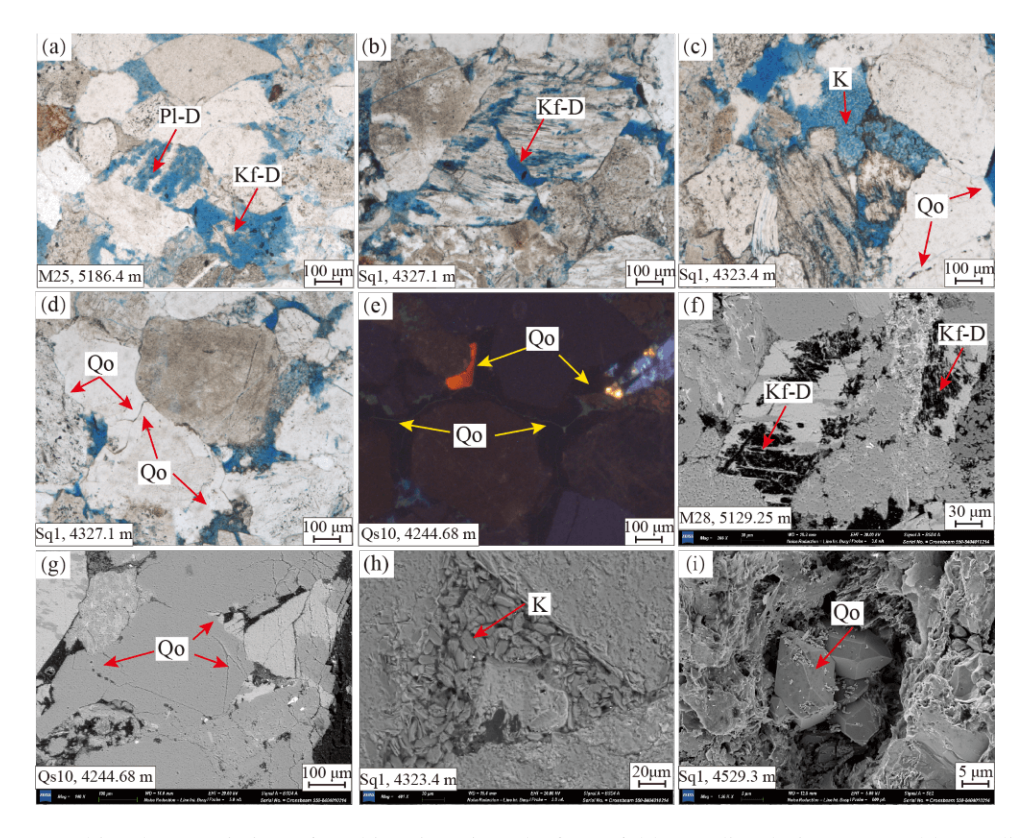


Fig. 4. Micropetrographic characteristics of authigenic minerals from feldspar dissolution. (a) Feldspar dissolution, (b) K-feldspar dissolution, (c) quartz overgrowth and authigenic kaolinite, (d) quartz overgrowth, (e) CL characteristics of quartz overgrowth, (f) K-feldspar dissolution (under SEM), (g) quartz overgrowth (under SEM), (h) authigenic kaolinite (under SEM) and (i) authigenic quartz (under SEM). Pl-D-plagioclase; Kf-D-K-feldspar dissolution; Al-D-albite dissolution; Qo-quartz overgrowth, K-kaolinite.

The point-counting data shows that the volume content of detrital quartz ranges from 21.3% to 38.4%, with an average of 28.15%, and the volume content of feldspar varies from 15.6% to 32.1%, with an average of 21.3%. Meanwhile, the volume content of rock fragment is between 38.5 to 60.9%, with an average of 50.54%. The rock fragment is mainly composed of volcanic and metamorphic rock fragments. Among the volcanic rock fragments, tuff fragments are the primary type, and for metamorphic rock fragments, quartzite and slate fragments are the dominant types. The sandstones are compositionally immature, which are classified as feldspathic lithic sandstone (Fig. 3(c)). Bulk XRD revealed that the mineral components are mainly composed of quartz, plagioclase, K-feldspar, and clay minerals, and a few samples contain a small amount of calcite, ferroan calcite and ankerite (Table S4).

3.2 Mineral diagenesis

3.2.1 Feldspar dissolution

Feldspar dissolution exhibits pronounced development within the Jurassic Badaowan Formation reservoirs of the Junggar Basin, particularly in coal-proximal intervals. The petrological analysis demonstrates the preferential dissolution of K-feldspar and albite components in tight sandstones (Figs. 4(a), 4(b) and 4(f)). This dissolution process has generated extensive secondary porosity systems, manifesting as three

distinct morphological types: (1) Embayed intergranular dissolution pores, (2) honeycomb-structured intragranular pores, and (3) isolated intragranular dissolution pores. A quantitative analysis of cast thin sections reveals measurable feldspar dissolution intensities ranging from 0.6% to 2.93%, with an average of 1.70% (Table S5). The dissolution-enhanced porosity networks significantly improve reservoir connectivity, particularly in zones influenced by coal-derived organic acid fluxes.

3.2.2 Authigenic quartz

Authigenic quartz constitutes the predominant cement type within the Badaowan Formation reservoirs. Petrographic analysis demonstrates two principal occurrence modes: (1) Syntaxial overgrowths on detrital quartz margins exhibiting characteristic optical continuity (Figs. 4(c) and 4(d)), and (2) pore-filling euhedral crystals observable via SEM imaging (Fig. 4(i)). CL microscopy reveals non-luminescent overgrowth zones forming concentric cementation halos around the detrital cores (Fig. 4(e)). These quartz cementation features progressively occlude intergranular porosity through radially developed overgrowths, which is particularly evident at the quartz-quartz grain contacts (Figs. 4(d) and 4(g)). The quantitative evaluation of thin sections establishes quartz overgrowth volumes ranging from 0.41% to 2.02% (Table S5), with spatial distribution controlled by sandstone texture and fluid flux

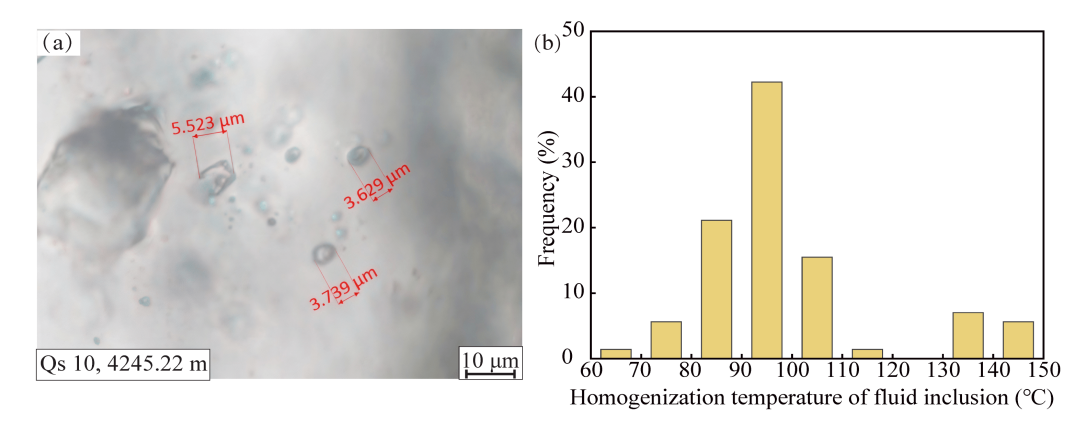


Fig. 5. (a) Fluid inclusion characteristics and and (b) the homogenization temperature distribution of quartz overgrowth, based on 70 measurements from 10 samples.

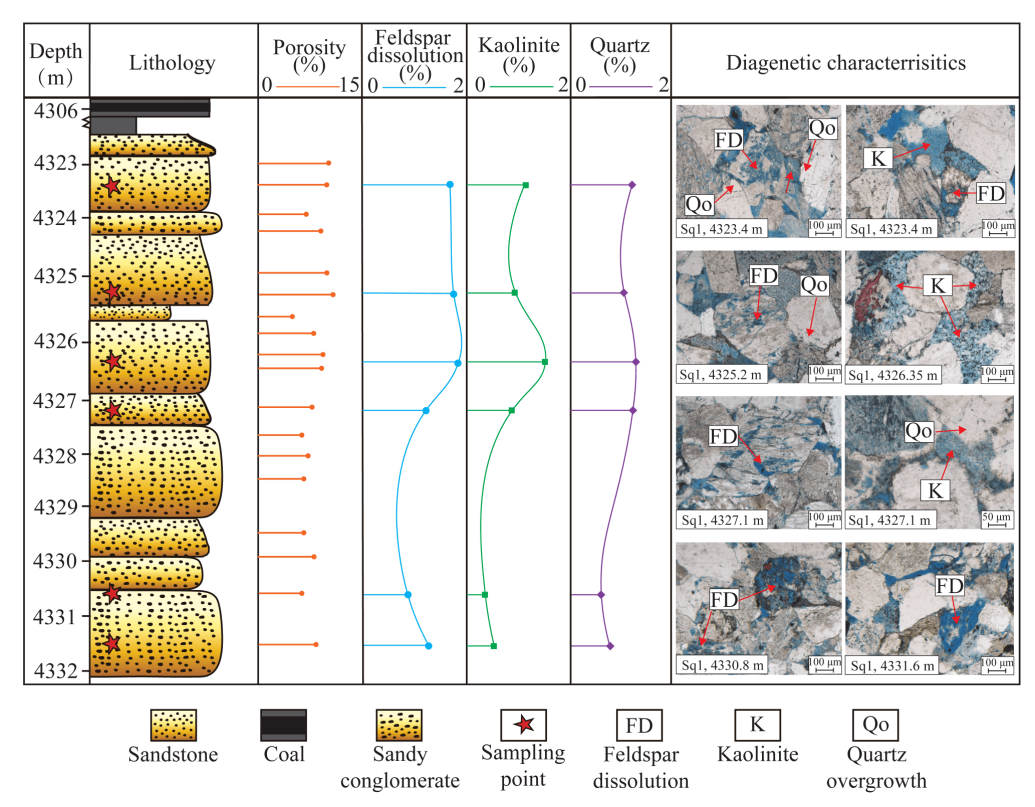


Fig. 6. Distribution characteristics of feldspar dissolution, kaolinite and quartz overgrowth. Distribution characteristics of feldspar dissolution and related authigenic minerals in Sq1 well.

history (Yuan et al., 2015). Fluid inclusion microthermometry provides critical constraints on the conditions of quartz cementation. Primary aqueous inclusions (3-9 μm) within overgrowths (Fig. 5(a) exhibit homogenization temperatures (Th) predominantly clustering between 80-110 °C, with subordinate populations at <80 °C and >120 °C (Fig. 5(b)). This Th distribution reflects the occurrence of multistage cementation events.

3.2.3 Clay minerals

Kaolinite dominates the clay mineral assemblage within the coal-measure tight sandstones of the Badaowan Formation, serving as a key diagenetic byproduct of feldspar dissolution with significant reservoir quality implications. Petrogenetic analysis demonstrates that feldspar alteration liberates silica and aluminum ions, precipitating authigenic kaolinite aggregates that preferentially occupy intergranular pores and dissolution pores (Figs. 4(c) and 4(h)). SEM reveals characteristic pseudohexagonal plates with well-developed crystal faces, indicative of crystallization under acidic porewater conditions (Fig. 4(h)). Quantitative petrographic data from thin sections reveal kaolinite volumes ranging from 0.32% to 1.88% (avg. 1.03%) (Table S5), and the vertical heterogeneity reflects material transport during deep diagenetic processes (Fig. 6) (Huang et al., 2025).

3.2.4 Distribution of feldspar dissolution and related authigenic minerals

The development of secondary porosity constitutes a critical factor controlling reservoir quality in coal-measure tight sandstone. The spatial characterization of feldspar dissolution and associated authigenic mineral distributions provides essential constraints for predicting high-permeability zones. In the reservoirs of the Badaowan Formation, feldspar dissolution intensities demonstrate strong coupling with the coal seam distribution, as evidenced by thin section analyses from Well Sq1. The sandstone proximal to coal seams exhibits enhanced dissolution features (Fig. 6), with dual coal-seam systems showing greater dissolution intensity compared to single coal seam adjacent reservoirs (Fig. S1). This spatial relationship implies coal-derived organic acid flux controlled by source proximity and fluid migration pathways (Barth and Riis, 1992). Quantitative mineral correlations reveal that the authigenic kaolinite and quartz overgrowth exhibit significant positive correlations with feldspar dissolution indices (Fig. S2), confirming their genetic linkage. However, lithofacies-controlled precipitation patterns show anomalous vertical zonation: Authigenic mineral contents (especially kaolinite) in coal-proximal facies (upper lithofacies) remain lower than mid-lithofacies equivalents, contrasting sharply with the feldspar dissolution-authigenic mineral precipitation distributions of non-coal measure reservoirs (Yuan et al., 2015). This relationship suggests that coalderived organic acids markedly enhance dissolution while inhibiting precipitation near the coal seam, creating distinct geochemical microenvironments along fluid migration paths (Zhang et al., 2021).

3.3 Result of react-transport models

3.3.1 Mineral saturation

The solubility index (SI) in PHREEQC quantitatively characterizes the mineral saturation states, with SI < 0 indicating undersaturation and SI > 0 denoting supersaturation. At 25 °C, feldspars (K-feldspar, albite, anorthite) deviate from equilibrium, with greater deviation at the 10 m/yr flow rate. The negligible upstream-downstream SI difference indicates the efficient transport of elements and Al-chelates under high flow conditions during the early diagenetic A stage (\sim 50 °C) (Figs. S3a and S3b).

In the model at 65 °C, there is an increase in the SI for feldspar (Fig. 7(a)). Upstream SI remains lower than downstream, highlighting the influence of oxalic acid chelation. A sharp midstream inflection point under 0.1 m/yr flow reflects restricted Al-chelate mobility and reduced solute transport at low velocities. Quartz remains undersaturated and kaolinite reaches saturation only in mid-downstream zones (Fig. 7(b)), suggesting that Al³⁺ and SiO₂(aq) concentrations remain below the precipitation thresholds even after 2,500 years. By 100 °C, the Al and Si concentrations rise markedly, elevating feldspar SI (Figs. 8(a) and 8(f)). High-temperature and lowflow rate conditions promote solute accumulation, reducing upstream-downstream SI gradients. Widespread quartz and kaolinite precipitation occurs (SI > 0; Fig. 8(b)), but ox-

alic acid chelation maintains kaolinite undersaturation at the sandstone-coal interfaces. In the 130 °C model, K-feldspar and albite approach equilibrium (Fig. S4(a)). Illite becomes stable in mid- and downstream regions, especially under low flow (0.001 m/yr), where its supersaturation correlates spatially with kaolinite undersaturation, confirming active illitization (Fig. S4(b)); meanwhile, higher quartz SI upstream indicates more extensive feldspar dissolution and limited Si transport in a nearly closed system (Fig. S4(b)).

3.3.2 Fluid pH

Fluid pH in the modeled system is governed by three principal factors: (1) H+ release through the dissociation of acetic and oxalic acids; (2) alkali metal ion liberation via mineral dissolution; (3) the flow rate of formation water. Under constant organic acid dissociation rates prescribed in the model, comparative simulations demonstrate that a high formation water flow rate can rapidly replace pore water, significantly altering the pH conditions of the diagenetic environment. For example, high-flow systems (10 m/yr) at the 25 °C model temperature maintain alkaline conditions (pH 8.26), whereas low-flow rate (1 m/yr) ones develop acidic environments (pH 4.52-4.55) (Fig. S3(d)). The influence of low rate becomes weaker below the flow rate of 0.1 m/yr, as evidenced by the diminishing pH variation shown in Figs. 7(e), 8(e) and S4(e). Concomitantly, a flow rate reduction amplifies longitudinal pH gradients, with upstream SI showing stronger acidity than downstream SI.

3.3.3 Changes in K, Na, Ca, Al, and Si concentrations

The concentrations of Al, Si, Na, Ca, and K in the models are primarily the result of feldspar dissolution, the precipitation of authigenic minerals, and mass transfer induced by dispersion. Specifically, the element concentration of the model is controlled by the dissolved amount of feldspar, and the distribution of element in space is determined by the mass transfer of fluid (Figs. S3(e), 7(f), 8(f), S4(f)). Elemental abundance patterns demonstrate strong temperature dependence; the concentration of Al at 130 °C is significantly higher than that in the model at 25 °C. (Figs. S3(e) and S4(f)). Numerical simulations demonstrate a flow rate dependence in the spatial distribution of Al and Si transport: For the high-flow rate model (e.g. 25 °C-10 m/yr model), Al and Si concentrations in downstream simulation cells exceed those in upstream cells. Conversely, for the low-flow rate model (e.g., 130 °C-0.001 m/yr model), upstream cells exhibit elevated Al and Si concentrations relative to downstream cells. This result indicates that molecular diffusion begins to dominate the mass transfer process at the flow rate of 0.001 m/yr, significantly reducing the scale of element mobilization (Maher, 2010).

3.3.4 Quantitative characterization of feldspar dissolution and authigenic mineral precipitation

Numerical simulations at 25 $^{\circ}$ C reveals that feldspar dissolution is limited, with average volumes of 1.38×10^{-4} cm³ (10 m/yr) and 1.01×10^{-2} cm³ (1 m/yr). (Fig. S3(c)). No authigenic mineral precipitates form, and feldspar dissolution can be completely transformed into secondary porosity [secondary

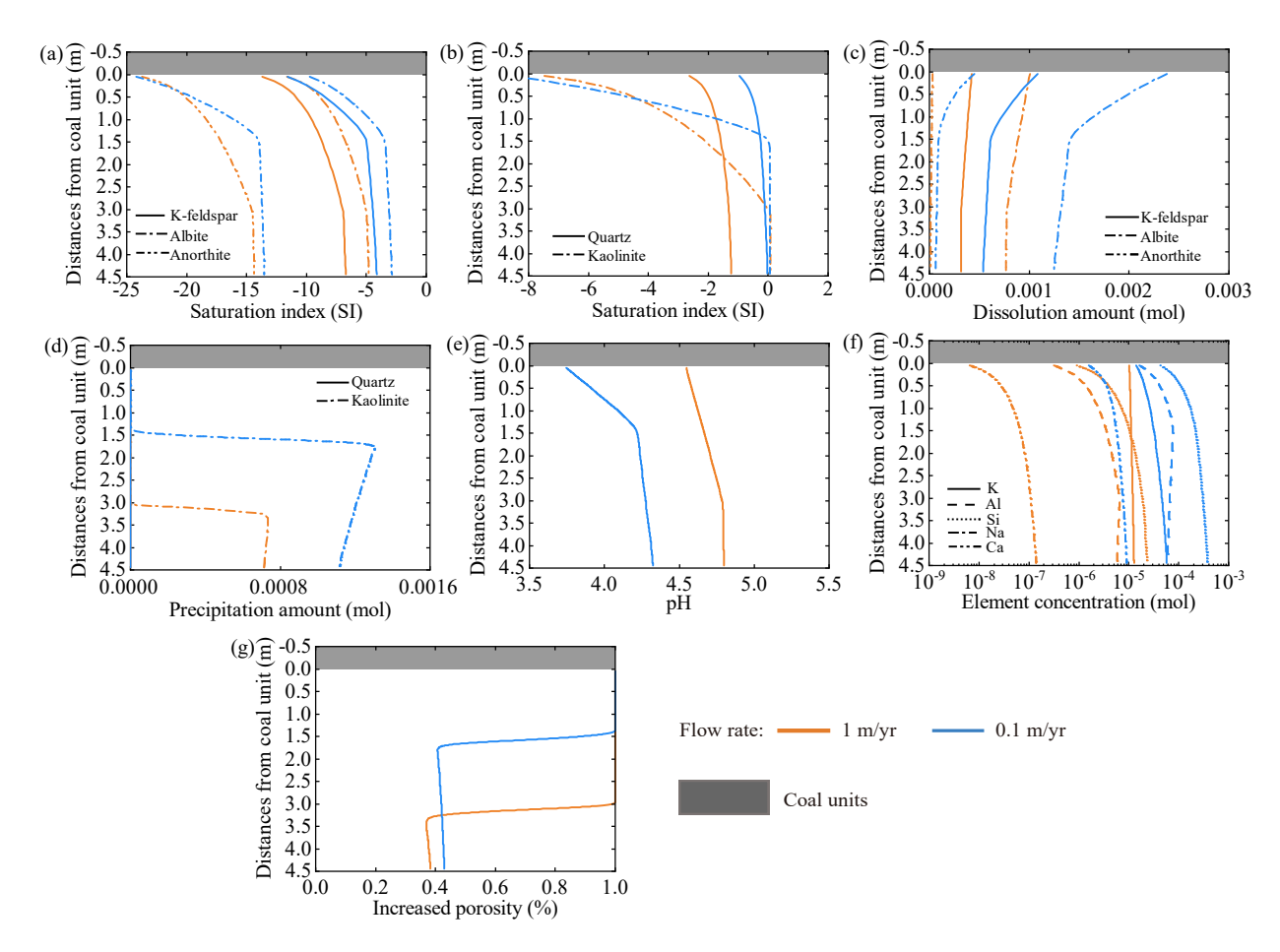


Fig. 7. Model outputs of (a)-(b) mineral saturation index, (c) dissolution amount, (d) precipitation amount (d), (e) pH, (f) element concentration and (g) increased porosity at 65 °C and flow rates of 1 and 0.1 m/yr.

porosity = (feldspar dissolved volume - authigenic mineral precipitation volume)/feldspar dissolved volume]. At 65 °C, dissolution increases significantly to 0.037 cm³ (1 m/yr) and 0.126 cm³ (0.1 m/yr), with the higher dissolution at lower flow rates linked to solution pH. Quartz and kaolinite precipitation under the 0.1 m/yr flow rate reduce the average secondary porosity to 62.14%, observed only in mid- and downstream cells (Figs. 7(d) and 7(g)). At 100 °C, dissolution volumes reach 0.94 cm³ (0.1 m/yr) and 0.69 cm³ (0.01 m/yr). A strong upstream dissolution preference is observed, with dissolution rates 2.44-8.29 times higher than downstream (Fig. 8(c)), which is attributed to oxalic acid chelation and limited mass transport. The analysis suggests that this spatial heterogeneity may not only be related to pH but also crucially influenced by the chelating effect of oxalic acid and the mass transfer of formation water. A detailed analysis will be provided in Section 4.1. Extensive precipitations of kaolinite and quartz are observed in Fig. 8(d). The average precipitation volumes of kaolinite are 0.45 cm^3 (0.1 m/yr) and 0.32 cm^3 (0.01 m/yr), and the average precipitation volumes of quartz are 0.004 cm³ (0.1 m/yr) and 0.11 cm³ (0.01 m/yr). Widespread kaolinite and quartz precipitation reduces secondary porosity, particularly downstream, where it ranges from 10.75-20.46% under 0.01 m/yr flow, compared to 33.25-95.53% upstream (Fig. 8(g)). At 130 °C, feldspar dissolution remains high (0.88 cm³ at 0.01 m/yr; 0.81 cm³ at 0.001 m/yr). Spatial disparities diminish under very low flow rate (0.001 m/yr), reflecting a restricted solute and Al-chelate transport (Fig. S4(c)). Kaolinite is partially replaced by illite, and enhanced feldspar dissolution and kaolinite illitization triggers substantial quartz precipitation, averaging 0.29 cm³ (0.01 m/yr) and 0.32 cm³ (0.001 m/yr). The maximum precipitation occurs at sandstone-coal interfaces (Fig. S4(d)). Secondary porosity drops to an average of 8.01%, with upstream secondary porosity ranging from 9.8% to 42.45% and downstream ranging from -0.03% to 0.59% under a flow rate of 0.001 m/yr (Fig. S4(g)).

4. Discussion

4.1 Mechanism of feldspar dissolution in coal-measure reservoir

Feldspar dissolution in geological systems is synergistically controlled by environmental physical factors and fluid chemical conditions (Fu et al., 2009; Crundwell, 2015). Within coal-measure strata, this process is intimately linked to coal-derived organic acids, where the production of these acids – particularly dicarboxylic species like oxalic acid – establishes critical geochemical prerequisites for effective feldspar disso-

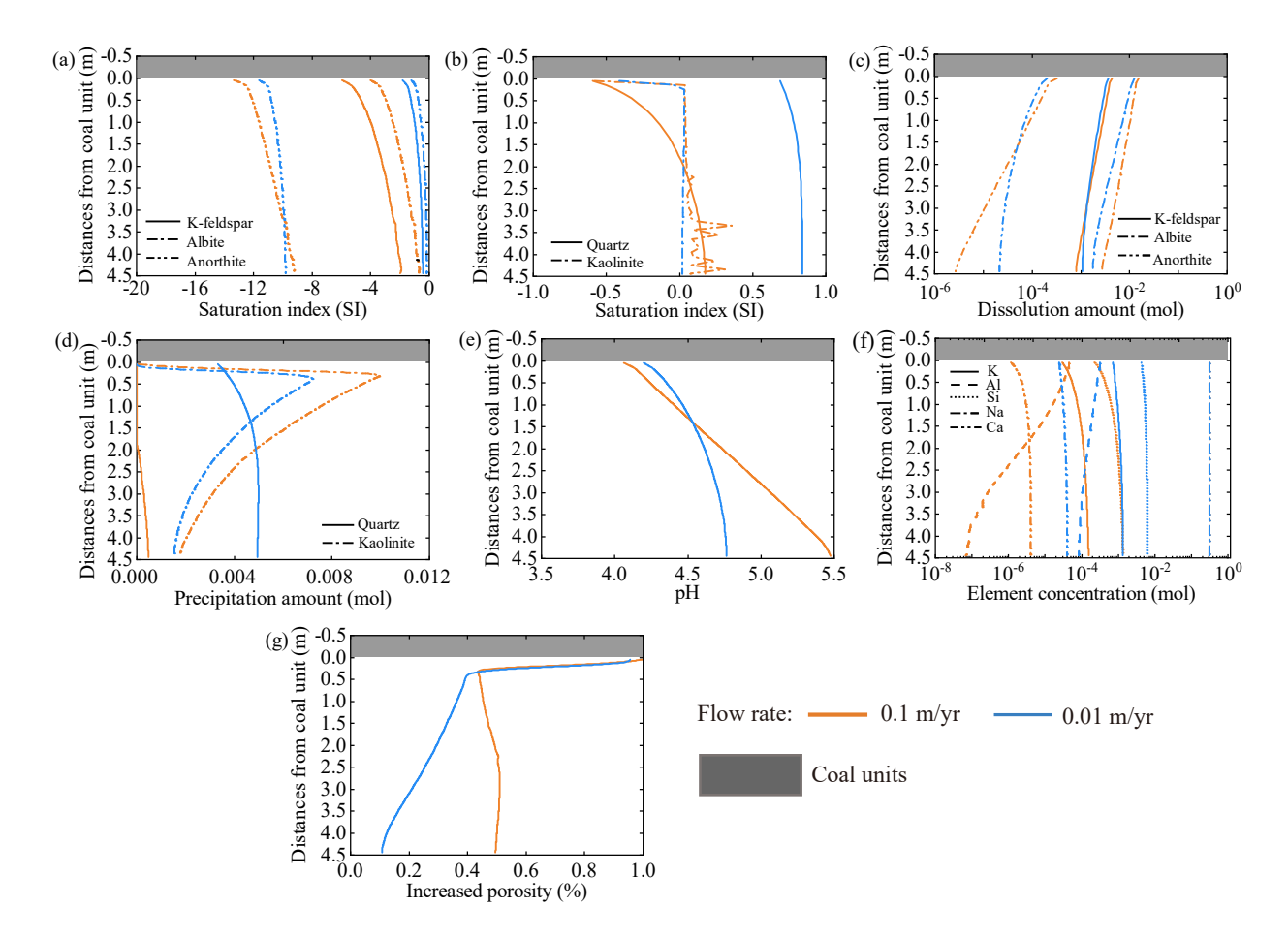


Fig. 8. Model outputs of (a)-(b) mineral saturation index, (c) dissolution amount, (d) precipitation amount, (e) pH, (f) element concentration and (g) increased porosity at 100 °C and flow rates of 0.1 and 0.01 m/yr.

lution (Lazo et al., 2017; Lin et al., 2020). The formation water flow rate exerts primary control over solute transport, while temperature modulates reaction kinetics through its direct influence on dissolution rate constants (Steefel and Lasaga, 1994; Schleicher et al., 2009). Our findings demonstrate that the Jurassic Badaowan Formation reservoirs exhibit a three-dimensional constraint mechanism, where organic acid generation, formation water flow rate, and temperature collectively govern the spatiotemporal evolution of feldspar dissolution.

4.1.1 Chelation of organic acid

The diagenetic evolution of coal strata generates a substantial amount of acetic and oxalic acids, representing a distinctive signature of coal-type kerogen decomposition (Kawamura and Kaplan, 1987; Li et al., 2021). Previous studies have demonstrated that oxalic acid has high H⁺ donation capacity and chelates aluminum to form strong multidentate chelates with high stability constants (Thomas et al., 1991; Welch and Ullman, 1993). The specific chelation equations and equilibrium constants are detailed in Table S2. In the feldspar dissolution reaction facilitated by oxalic acid, the formation of Al-oxalate chelates (e.g., $Al(C_2O_4)^{2^-}$, $Al(C_2O_4)^{3^-}$) can effectively reduce aqueous inorganic Al activity in the fluid, maintaining the SI of feldspars in the fluid away from

equilibrium and sustaining dissolution kinetics (Surdam and MacGowan, 1987; Cama and Ganor, 2006; Zhang et al., 2009; Marsala and Wagner, 2016). To clarify the impact of oxalic acid chelation on feldspar dissolution, this study established a comparative model using identical conditions for temperature, flow rate, mineral reaction rates, and reaction equilibrium constants, with oxalic acid as the sole variable in the model. The simulation results show that as the concentration of oxalic acid increases, feldspar dissolution undergoes a significant enhancement (Figs. 9(a)-9(c)). Comparative analysis shows that the average dissolution amount of K-feldspar in the 30% oxalic acid model rises by 14.72% compared to the model with 10% oxalic acid (Fig. 9(a)). Among these cells, the upstream 15 simulation cells exhibit a dissolution increment ranging from 14.19% to 35.82%, and that of the downstream 15 simulation cells is minor with an increase of $12.10\% \sim 12.74\%$. Similarly, albite and anorthite has similar dissolution characteristics. Compared with the Al concentration in the simulation results, total Al concentration in the solution gradually increases with the augmentation of oxalic acid content (Fig. 10(a)), indicating that the concentration of organic aluminum in the solution increases significantly and the mineral saturation of feldspar in the solution exhibits a relative decrease. This result is closely aligned with the complexation model derived from laboratory experiments by Cama and Ganor (2006). Furthermore, the

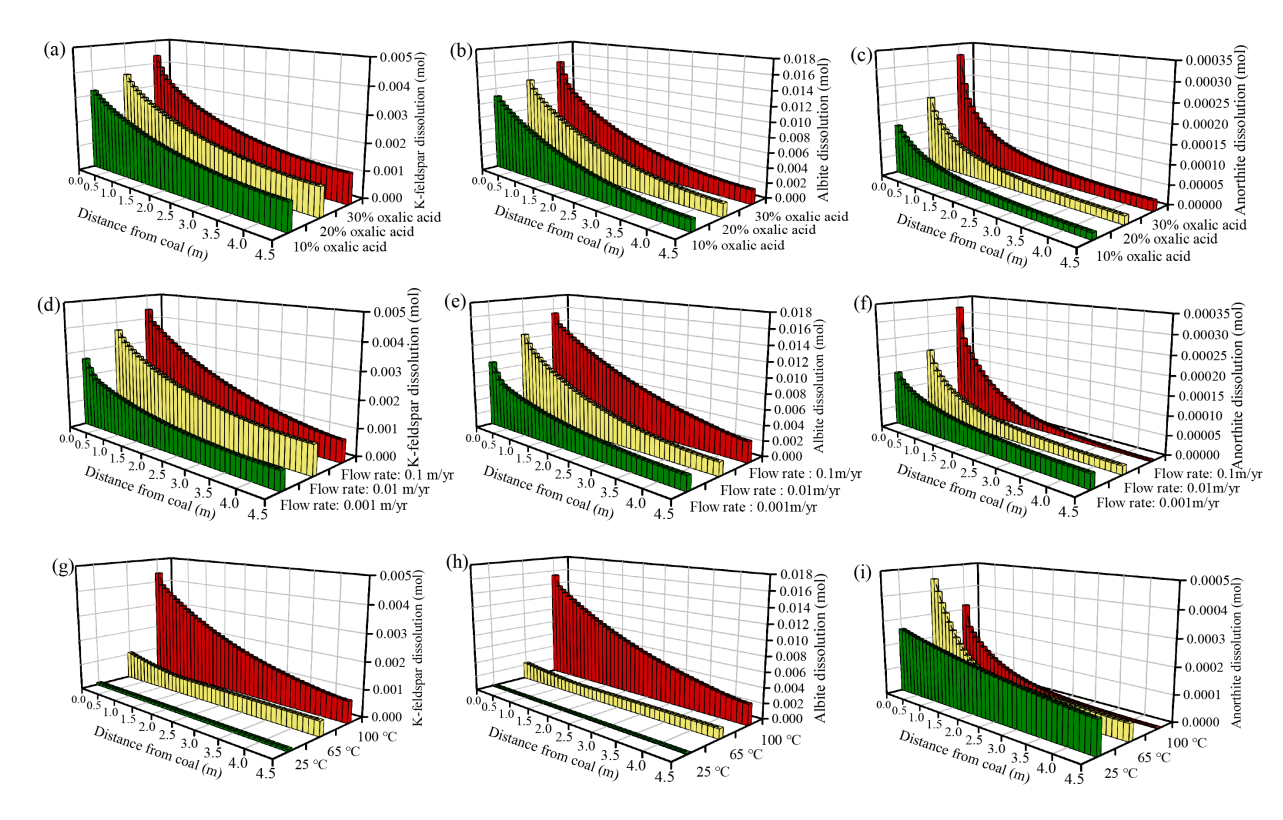


Fig. 9. Feldspar dissolution characteristics with the constraints of oxalate, flow rate and temperature. Dissolution characteristics of (a) K-feldspar, (b) albite, (c) anorthite with various oxalic acid concentrations at a temperature of 100 °C and a flow rate of 0.01 m/yr; (d) dissolution characteristics of K-feldspar, (e) albite, (f) anorthite with different formation-water flow rates at 100 °C; (g) dissolution characteristics of K-feldspar, (h) albite and (i) anorthite at various temperatures and a flow rate of 0.1 m/yr.

pH of the solution also declines with increasing oxalic acid concentration (Fig. 10(b)). The comprehensive analysis reveals that the effect of dissolution enhancement is strongest in the upstream, followed by the midstream, and weakest in the downstream.

4.1.2 Formation water flow rate

The evolution of formation water flow rates in sedimentarydiagenetic systems exhibits a decline from shallow (high flow rate/open) to deep (low flow rate/closed) diagenetic environments, fundamentally affecting feldspar dissolution kinetics (Giles, 1987; Thyne, 2001). The low-temperature model (25 °C) shows that the amounts of feldspar dissolution in the model of 10 m/yr flow rate are less than that in the model of 1 m/yr flow rate, and the pH in the model of 10 m/yr flow rate is significantly higher in the model with 1 m/yr, indicating that the flow rate influences feldspar dissolution by constraining the pH of fluids in open diagenetic systems (Fig. S3(d)). In deep, high-temperature environments (100) °C) characterized by low flow rates (0.001-0.1 m/yr), our simulations provide critical evidence for the model where solute transport becomes the limiting factor (Yuan et al., 2017; Bjørlykke and Jahren, 2012; Steefel and Maher, 2009). The results reveal that ultra-low flow conditions (0.001 m/yr) suppress dissolution by 39.22% (K-feldspar) and 49.14% (albite) relative to the 0.1 m/yr benchmark, also significantly reducing anorthite dissolution upstream (Figs. 9(d) and 9(f)). Concurrently, Al and Si concentrations exhibit inverse flow rate dependence, and the change in Al concentration is more significant (Figs. 10(c) and 10(d)). These results reveal that the transfer limitation elevates feldspar SI through solute retention, driving the diagenetic system toward chemical equilibrium and consequent dissolution inhibition.

4.1.3 Temperature

Temperature exerts an influence on the kinetic rate of feldspar dissolution by governing the reaction rate constant (Zhang et al., 2009; Yuan et al., 2019). Comparative models indicate that the amounts of feldspar dissolution increase significantly with rising temperature, and the dissolution difference tends to enlarge from the upstream to the downstream (Figs. 9(g)-9(i)). Comparing the 100 °C model to the 25 °C model, the K-feldspar dissolution increases by 9.54-42.92 times, the albite dissolution increase ranges from 28.84 to 130.17 times, while the anorthite dissolution is inhibited. The analysis indicates that kinetic dominance triggers dramatic dissolution enhancements for K-feldspar and albite under 100 °C conditions. In contrast, anorthite dissolution at low temperature is more advantageous mainly due to its lower activation energy $(\Delta E = 16.60 \text{ kJ/mol})$ and higher Al/Si ratio (Zhang et al., 2009; Yang et al., 2014). However, the extensive dissolution of K-feldspar and albite during diagenetic heating drives fluid-

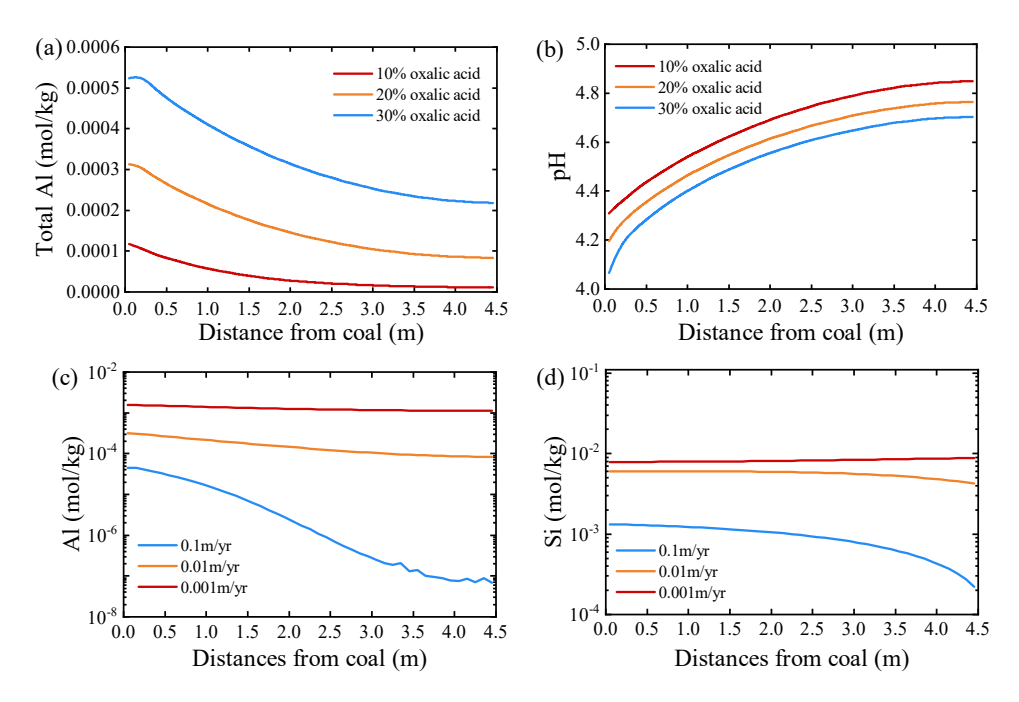


Fig. 10. Al and Si concentration of solution of different flow rates in 100 °C models.

phase feldspar saturation toward equilibrium, while the limited reactive surface area of anorthite by its smaller proportion (5%) constrain its dissolution capacity within the simulated system (Chou and Wollast, 1984; Yuan et al., 2019).

4.2 Authigenic mineral precipitation is constrained by mass transfer

The mass transfer of fluids governs the precipitation of authigenic minerals in sandstone. During the transformation of sediment to consolidated rock, both the environmental physical factors and fluid chemical factors of the diagenetic system significantly influence the precipitation and distribution of authigenic minerals (Zhu et al., 2010).

4.2.1 Precipitation characteristics of authigenic minerals

React-transport models demonstrate systematic controls of temperature, organic acid and system openness (flow rate) on the precipitation of authigenic minerals across four stages. In the 25 °C open system, authigenic precipitation is nonexistent due to the rapid solute transfer, forming complete secondary porosity (Fig. S3(b)). In the 65 °C semi-opened system, early precipitation of kaolinite is observed at the midstream to downstream cells in the models (Fig. 7(d)). In the 100 °C semi-closed system, kaolinite and quartz precipitate extensively and abundantly. The peak of kaolinite precipitation occurs in the upstream, while the kaolinite in several cells near the coal units remains suppressed (Fig. 8(d)). The peak of quartz precipitation is distributed in the midstream of the model, and quartz precipitation in the upstream is lower than that in the midstream and downstream (Fig. 8(d)). In the 130 °C near-closed system, there is a positive correlation between the dissolution of kaolinite, quartz and feldspar (Fig. S4(d)). Under the flow rate condition of 0.001 m/yr, kaolinite illitization is observed in downstream and illite precipitation,

showing a gradual increase towards the downstream direction (Fig. S4(d)).

4.2.2 Controlling factors of authigenic mineral precipitation

The reaction kinetics of mineral dissolution are predominantly governed by temperature (Palandri and Kharaka, 2004). Elevated temperatures accelerate feldspar dissolution rates, progressively increasing Al3+ and SiO₂(aq) concentrations until reaching the equilibrium thresholds for quartz and kaolinite precipitation. Notably, the geochemical prerequisites for kaolinite and quartz precipitation exhibit fundamentally distinct temperature dependencies. The concentrations of Al³⁺ and SiO₂(aq) required for kaolinite precipitation gradually decrease with rising temperature, and the concentration of SiO₂(aq) required for quartz precipitation increases with increasing reaction temperature. Moreover, the SiO₂(aq) required for kaolinite precipitation is much lower than that of quartz at the same temperature (Yuan et al., 2017; Cao et al., 2022). This differential precipitation mechanism results in the precipitation of only kaolinite in the semi-open model with low solute concentration (Fig. S4(d)). Progressive temperature increases enhance the feldspar dissolution efficiency, elevating solute concentrations in the fluid phase and consequently expanding the precipitation domains of both authigenic minerals (Zhu and Lu, 2009).

The formation water flow rate critically controls the solute concentration. Comparative modeling at each temperature condition demonstrates that flow rates exert fundamental control on authigenic mineral distribution. The simulation results reveal an inverse correlation between flow rate and authigenic mineral, with both kaolinite and quartz precipitation amounts and spatial extent markedly enhanced under reduced flow rates (Figs. 7(d), 8(d) and S4(d)), indicating that the flow rate controls the distribution and precipitation amount of authi-

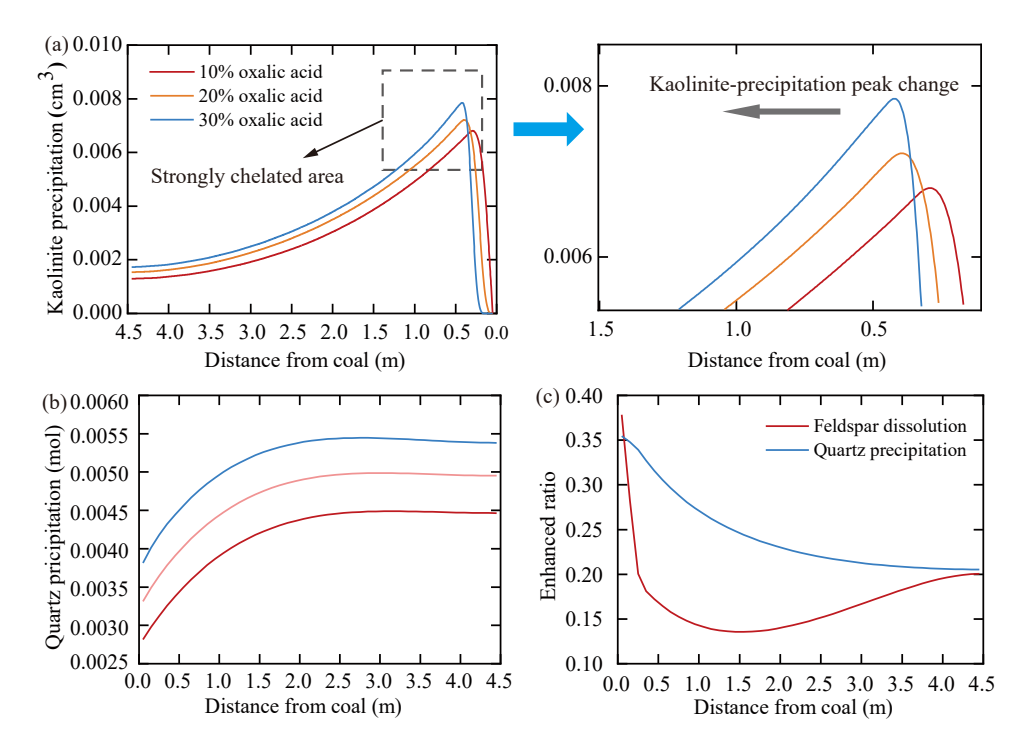


Fig. 11. Precipitation characteristics of (a) kaolinite, (b) quartz in models with different oxalic acid concentrations under conditions of 100 °C and a flow rate of 0.01 m/yr and (c) the enhanced ratio of total feldspar dissolution volume and quartz precipitation volume was compared.

genic minerals by transporting solutes (Giles, 1987; Steefel and Maher, 2009). In high flow rate simulations, high flow rate enables long-distance solute transport, thereby inhibiting authigenic mineral precipitation, as evidenced in 25 °C models with 10 and 1 m/yr flow rates (Fig. S3). Additionally, the flow rate is extremely slow, such as 0.001 m/yr at 130 °C, when molecular diffusion takes control over solute transfer, limiting the long-distance transport of authigenic minerals and resulting in kaolinite and quartz precipitate in situ (Fig. S4(d)). Changes in the flow rate from high to low significantly influence the spatial matching relation between authigenic quartz and feldspar dissolution. At a relatively high flow rate, solutes are partially transported away, resulting in low quartz precipitation in extensive feldspar dissolution zones and high quartz cementation in weaker feldspar dissolution zones. At the low flow rate condition, molecular diffusion leads to in-situ quartz precipitation, forming the general geological phenomenon of extensive feldspar dissolution accompanied by abundant authigenic quartz. Notably, the direct influence of flow rate on the distribution of kaolinite precipitation is relatively small from 65 to 130 °C (Yuan et al., 2017). Illitization processes exhibit analogous flow-dependence, with reduced flow rates enhancing the illite precipitation potential (Fig. S4(d)). This behavior stems from the elevated diffusivity of potassium (Huang et al., 2009; Thyne, 2001), which promotes downstream K⁺ accumulation and the consequent intensification of kaolinite-illite transformation reactions.

Organic chelation, particularly through oxalic acid, exerts significant control over authigenic mineral precipitation. The comparative analysis of authigenic mineral precipitation in

100 °C-0.01 m/yr models with varying oxalic acid concentrations demonstrates that Al-oxalate chelates formation suppresses aqueous Al3+ concentrations in cells adjacent to the coal, simultaneously enhancing feldspar dissolution rates and inhibiting kaolinite precipitation (Fig. 11(a)) (Harrison and Thyne, 1992; Blake and Walter, 1999). This chelationdriven process substantially enhances Al transport in diagenetic systems and facilitates secondary porosity development (Fig. 7(g), 8(g) and S4(g)). The influence of this mechanism is particularly significant in the low-temperature model (65 °C), where kaolinite precipitation peaks are abnormally distributed in the middle of the lithofacies (Fig. 7(d)). This result is significantly different from the distribution characteristics of kaolinite precipitation in non-coal-measure sandstone (Yuan et al., 2017). These simulation results provide mechanistic explanations for the observed spatial decoupling between authigenic kaolinite distribution and feldspar dissolution zones in natural sandstone reservoirs (Fig. 6). Notably, the simulated Al mobilization exhibits limited spatial propagation (< 1 m scale) under the conditions of 100 °C-0.01 m/yr (Fig. 11(a)), contrasting with the wider unbalanced patterns observed in coal-measure sandstones. This result indicates that the precipitation kinetics of kaolinite are significantly constrained by temperature. Furthermore, thermal maturation studies indicate that peak dicarboxylic acid concentrations occur at 60-100 °C prior to decarboxylation thresholds (Surdam and MacGowan, 1987). In this temperature range, the diagenetic environment has undergone a transition from semi-open to closed. Thus, this unbalanced pattern of feldspar dissolution and kaolinite precipitation may form a ligand-mediated semi-

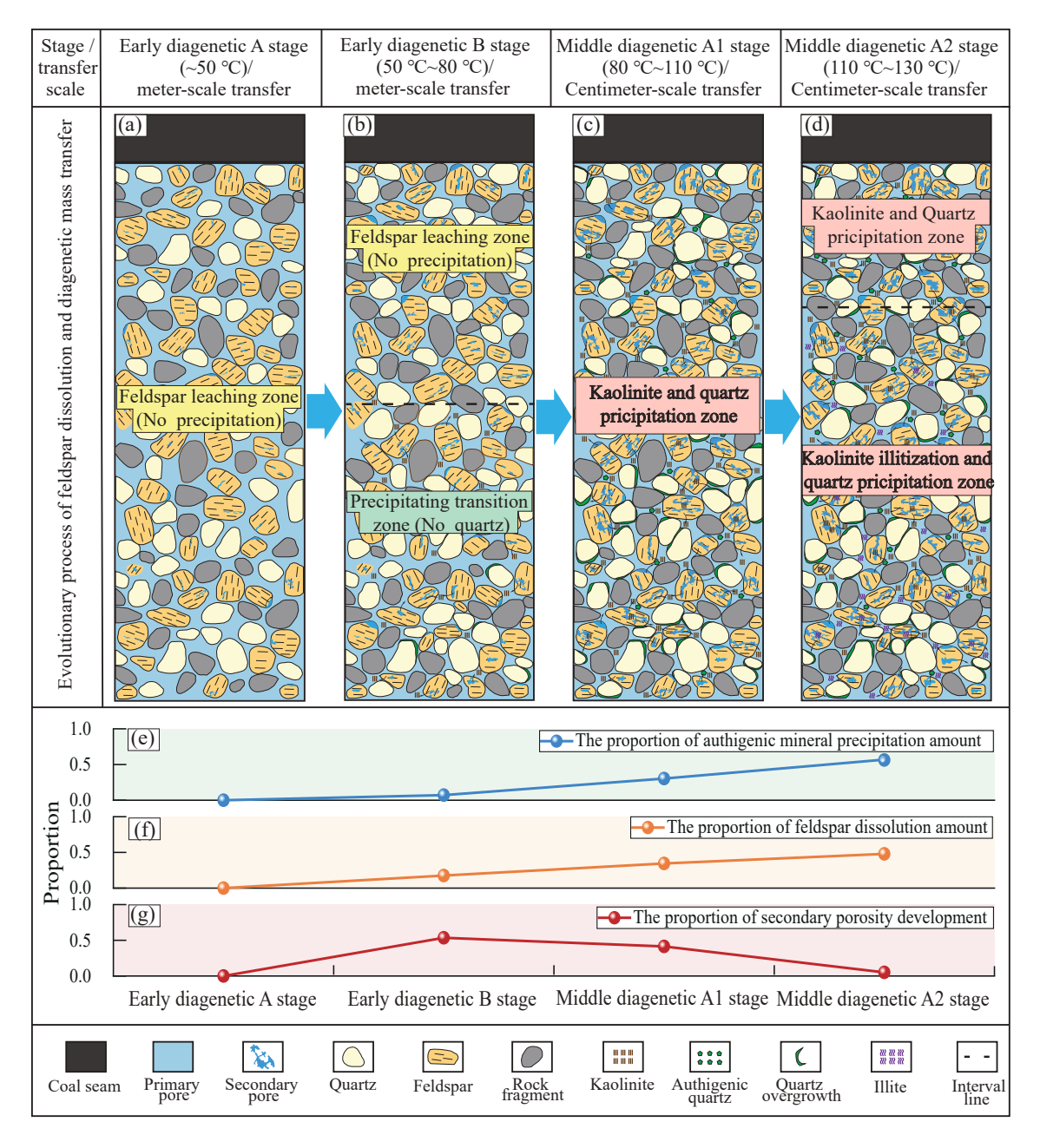


Fig. 12. (a)-(d) Evolutionary model of feldspar dissolution and authigenic mineral precipitation in sandstone-coal lithofacies combinations and (e)-(g) the proportions of dissolution, precipitation and secondary porosity formation at different evolutionary stages.

open and relatively low-temperature (< 100 °C) environment. As the concentration of oxalic acid increases, the amount of quartz precipitation significantly rises (Fig. 11(b)). To eliminate the influence of feldspar solubilization, the enhanced ratios of feldspar solubilization and quartz precipitation were calculated, and the results showed that the enhancement ratio of quartz precipitation is much higher than the feldspar solubilization (Fig. 11(c)). This implies that chelation-induced kaolinite suppression generates silicon supersaturation that, under closed-system transport limitations, drives quartz cementation as a silica-buffering mechanism.

4.3 Impact of feldspar dissolution and precipitation of authigenic minerals

Based on petrographic observations and insights from diagenetic numerical simulations, this study develops a process-based model (Fig. 12) to unravel the intrinsic mechanisms and spatial patterns of key diagenetic processes—particularly those involving organic acid-associated reaction-transport. The model aims to clarify the coupling mechanisms between feldspar dissolution and authigenic mineral precipitation, as well as their controls on reservoir quality, within coal-bearing tight sandstones. The analytical results demonstrate enhanced feldspar dissolution in coal-proximal sandstone units due to

organic acid enrichment. Notably, sandstone reservoirs with multiple coal seams exhibit significantly greater feldspar dissolution compared to single coal seam (Fig. S1), corroborating the critical role of coal-derived organic acids in dissolution processes. Quantitative modeling reveals two principal phases of secondary porosity development: The early diagenetic stage B (50-80 °C) and the middle diagenetic stage A1 (80-110 °C) (Figs. 12(b), 12(c) and 12(g)). The homogenization temperatures of fluid inclusions ranging from 60 to 80 °C in quartz overgrowths provide evidence for the precipitation of authigenic quartz during the early diagenetic stage B. Moreover, the low amount of fluid inclusions in this temperature range also suggests that high flow rate promotes solute transfer and extensive secondary porosity formation. The dense clustering of fluid inclusions within the 90-110 °C homogenization temperature range demonstrates three critical diagenetic constraints (Fig. 5(b)): (1) Extensive feldspar dissolution during the middle diagenetic stage A1; (2) silicasaturated pore fluid conditions; (3) a closed diagenetic system. Although the feldspar dissolution can be entirely converted into secondary porosity during the early diagenetic stage A (< 50 °C), the kinetic constraints at low temperatures substantially restrict dissolution efficiency (Fig. 12(a)). During the middle diagenetic stage A2 (110-150 °C; Cao et al., 2022), the feldspar dissolution reaches its peak, but the reservoir becomes extremely closed with kaolinite and quartz precipitating nearly in situ (Fig. 12(d)), suppressing secondary porosity development (Fig. 12(e) and 12(f)). In addition, the solute migration promoted by organic acid chelation leads to the formation of extensive feldspar dissolution and a small amount of kaolinite precipitation in sandstone that is close to the coal seam, which provides a prerequisite for the formation of highquality reservoirs in coal-bearing sandstone.

5. Conclusions

This study integrates petrographic analysis with reactiontransport modeling to elucidate the mechanisms controlling feldspar dissolution and authigenic mineral precipitation in coal-measure tight sandstones. The key findings are summarized as follows:

- Numerical simulations quantitatively demonstrate that organic chelation by oxalic acid is the key driver behind the observed spatial decoupling between feldspar dissolution and kaolinite precipitation. This explains the observed distinctive pattern that feldspar dissolution is intensified in sandstones proximal to coal seams (further enhanced in formations with multiple coal seams), and the resultant authigenic kaolinite are often suppressed in these same zones.
- 2) The model results quantitatively define the principal diagenetic stages for effective secondary porosity generation as being from the early diagenetic stage B (50-80 °C) to the middle diagenetic stage A1 (80-110 °C). A key insight is that while feldspar dissolution intensifies at higher temperatures (e.g., 130 °C), the system becomes transport-limited, resulting in significant *in-situ* authigenic precipitation and a drastically reduced effective

- secondary porosity.
- Organic acid, temperature and flow rate are the key controls on feldspar dissolution and authigenic mineral precipitation in coal-measure tight sandstones. Oxalic acid enhances the proton-promoting dissolution by reducing the pH of the fluid and forms Al-oxalate chelates to reduce feldspar mineral saturation in the solution as well as to facilitate feldspar dissolution. The formation water flow rate regulates dissolution processes through its dual effects on pH modulation and mineral saturation in pore fluids. Temperature exerts differential controls on feldspar dissolution: While K-feldspar and albite dissolution exhibit distinct thermal responses, anorthite dissolution becomes predominantly limited by aluminosilicate saturation equilibria at elevated temperatures. Additionally, temperature mediates the amount of authigenic mineral precipitation, coupled with the formation water flow rate, thus governing the spatiotemporal zoning patterns of authigenic kaolinite and quartz during diagenetic evolution. The chelation of aluminum by oxalic acid promotes the Al mobilization and facilitates the formation of secondary porosity. Under conditions suppressing kaolinite precipitation, quartz precipitation acts as a geochemical buffer to maintain solution saturation balance, resulting in the characteristic mineral assemblage distributions observed in coal-measure reservoirs.

In summary, this study provides a quantitative, processoriented framework that explains the mechanism of the formation of key diagenetic patterns in coal-measure tight sandstones. Through an enhanced understanding of the spatial decoupling of feldspar dissolution and authigenic minerals, the quantitative porosity window, and the operative mechanisms of organic acids, temperature, and flow rate, our knowledge of the mechanisms governing secondary porosity evolution in coal-measure sandstone reservoirs is significantly improved.

Acknowledgements

This study was supported by the National Natural Science Foundation of China (No. 42522204) and National Science and Technology Major Project of China (No. 2025ZD1402807). We would like to thank CNPC Xinjiang Oilfield Company for providing core samples and geological data of the Jurassic Badaowan Formation in the Junggar Basin.

Supplementary file

https://doi.org/10.46690/ager.2025.10.05

Conflict of interest

The authors declare no competing interest.

Open Access This article is distributed under the terms and conditions of the Creative Commons Attribution (CC BY-NC-ND) license, which permits unrestricted use, distribution, and reproduction in any medium, provided the original work is properly cited.

References

- Andresen, B., Throndsen, T., Barth, T., et al. Thermal generation of carbon dioxide and organic acids from different source rocks. Organic Geochemistry, 1994, 21(12): 1229-1242.
- Barclay, S. A., Worden, R. H. Geochemical modelling of diagenetic reactions in a sub-arkosic sandstone. Clay Minerals, 2000, 35(1): 57-67.
- Barth, T., Riis, M. Interactions between organic acids anions in formation waters and reservoir mineral phases. Organic Geochemistry, 1992, 19(4-6): 455-482.
- Bennett, P., Siegel, D. I. Increased solubility of quartz in water due to complexing by organic compounds. Nature, 1987, 326(6114): 684-686.
- Bevan, J., Savage, D. The effect of organic acids on the dissolution of K-feldspar under conditions relevant to burial diagenesis. Mineralogical Magazine, 1989, 53(372): 415-425.
- Bjørlykke, K., Jahren, J. Open or closed geochemical systems during diagenesis in sedimentary basins: Constraints on mass transfer during diagenesis and the prediction of porosity in sandstone and carbonate reservoirs. AAPG Bulletin, 2012, 96(12): 2193-2214.
- Blake, R. E., Walter, L. M. Kinetics of feldspar and quartz dissolution at 70-80 °C and near-neutral pH: Effects of organic acids and NaCl. Geochimica et Cosmochimica Acta, 1999, 63(13-14): 2043-2059.
- Blake, R. E., Walter, L. M. Effects of organic acids on the dissolution of orthoclase at 80 °C and pH 6. Chemical Geology, 1996, 132(1-4): 91-102.
- Boudreau, B. P. The diffusive tortuosity of fine-grained unlithified sediments. Geochimica et Cosmochimica Acta, 1996, 60(16): 3139-3142.
- Burgos-Cara, A., Putnis, C. V., Ortega-Huertas, M., et al. Influence of pH and citrate on the formation of oxalate layers on calcite revealed by *in situ* nanoscale imaging. Crystengcomm, 2017, 19(25): 3420-3429.
- Cama, J., Ganor, J. The effects of organic acids on the dissolution of silicate minerals: A case study of oxalate catalysis of kaolinite dissolution. Geochimica et Cosmochimica Acta, 2006, 70(9): 2191-2209.
- Cao, Y., Yuan, G., Wang, Y., et al. Successive formation of secondary pores via feldspar dissolution in deeply buried feldspar-rich clastic reservoirs in typical petroliferous basins and its petroleum geological significance. Science China Earth Sciences, 2022, 65(9): 1673-1703.
- Chou, L., Wollast, R. Study of the weathering of albite at room temperature and pressure with a fluidized bed reactor. Geochimica et Cosmochimica Acta, 1984, 48 (11): 2205-2217.
- Crundwell, F. K. The mechanism of dissolution of the feldspars: Part II dissolution at conditions close to equilibrium. Hydrometallurgy, 2015, 151: 163-171.
- Dong, S., Liu, L., Zhang, J., et al. Insight into the structures and reactivities of aqueous Al (III)-carboxylate complexes from cluster-based ab initio computational studies-Implications for the ligand-promoted mineral dissolution

- mechanism. Geochimica et Cosmochimica Acta, 2019, 244: 451-466.
- Folk, R. L. Petrology of Sedimentary Rocks. Austin, USA, Hemphill Publishing Company, 1974.
- Fu, Q., Lu, P., Konishi, H., et al. Coupled alkali-feldspar dissolution and secondary mineral precipitation in batch systems: 1. New experiments at 200 °C and 300 bars. Chemical Geology, 2009, 258(3-4): 125-135.
- Gao, C., Ji, Y., Gao, Z., et al. Multi-factor coupling analysis on property preservation process of deep buried favorable reservoir in hinterland of Junggar Basin. Acta Sedimentologica Sinica, 2017, 35(3): 577-591. (in Chinese)
- Gao, Z., Feng, J., Cui, J., et al. Physical simulation and quantitative calculation of increased feldspar dissolution pores in deep reservoirs. Petroleum Exploration and Development, 2017, 44(3): 387-398.
- Giles, M. R. Mass transfer and problems of secondary porosity creation in deeply buried hydrocarbon reservoirs. Marine and Petroleum Geology, 1987, 4(3): 188-204.
- Giles, M. R., De Boer, R. B. Origin and significance of redistributional secondary porosity. Marine and Petroleum Geology, 1990, 7(4): 378-397.
- Harouiya, N., Oelkers, E. H. An experimental study of the effect of aqueous fluoride on quartz and alkali-feldspar dissolution rates. Chemical Geology, 2004, 205(1-2): 155-167.
- Harrison, W. J., Thyne, G. D. Predictions of diagenetic reactions in the presence of organic acids. Geochimica et Cosmochimica Acta, 1992, 56(2): 565-586.
- He, Z., Shao, L., Kang, Y., et al. Analyzsis in Controls of the Coal Accumulation in the Jurassic Badaowan Formation, Junggar Basin. Acta Sedimentologica Sinica, 2004, 22: 449-454. (in Chinese)
- Hellevang, H., Pham, V. T., Aagaard P. Kinetic modelling of CO₂-water-rock interactions. International Journal of Greenhouse Gas Control, 2013, 15: 3-15.
- Huang, S., Huang, K., Feng, L., et al. Mass exchanges among feldspar, kaolinite and illite and their influences on secondary porosity formation in clastic diagenesis-A case study on the Upper Paleozoic, Ordos Basin and Xujiahe Formation, Western Sichuan Depression. Geochimica, 2009, 38(5): 498-506. (in Chinese)
- Huang, X., Guo, F., Ding, X., et al. Dissolution behavior of feldspar in oxalic acid at 40-100 °C: Implications for Al enrichment during chemical weathering. Solid Earth Sciences, 2025, 10(1): 100201.
- Kampman, N., Bickle, M., Becker, J., et al. Feldspar dissolution kinetics and Gibbs free energy dependence in a CO₂-enriched formation-water system, Green River, Utah. Earth and Planetary Science Letters, 2009, 284(3-4): 473-488.
- Kawamura, K., Kaplan, I. R. Dicarboxylic acids generated by thermal alteration of kerogen and humic acids. Geochimica et Cosmochimica Acta, 1987, 51(12): 3201-3207.
- Köhler, S. J., Dufaud, F., Oelkers, E. H. An experimental study of illite dissolution kinetics as a function of pH from 1.4 to 12.4 and temperature from 5 to 50 °C. Geochimica et Cosmochimica Acta, 2003, 67(19): 3583-3594.

- Lawrence, C., Harden, J., Maher, K. Modeling the influence of organic acids on soil weathering. Geochimica et Cosmochimica Acta, 2014, 139: 487-507.
- Lazo, D. E., Dyer, L. G., Alorro, R. D. Silicate, phosphate and carbonate mineral dissolution behaviour in the presence of organic acids: A review. Minerals Engineering, 2017, 100: 115-123.
- Li, H., Black, J. R., Hao, Y., et al. Modelling diagenetic reactions and secondary porosity generation in sandstones controlled by the advection of low-molecular-weight organic acids. Basin Research, 2024, 36(2): e12860.
- Li, P., Zhou, S., Zhang, X., et al. Distributions and evolution model of water-soluble organic acids for coals with different thermal maturations. Fuel, 2021, 283: 118863.
- Li, Y., Gao, X., Meng, S., et al. Diagenetic sequences of continuously deposited tight sandstones in various environments: A case study from upper Paleozoic sandstones in the Linxing area, eastern Ordos basin, China. AAPG Bulletin, 2019, 103(11): 2757-2783.
- Lin, H., Ning, F., Su, G., et al. The genetic mechanism and petroleum significance of Chepaizi-Mosuowanpaleo-uplift in the central Junggar Basin. Acta Petrologica Sinica, 2022, 38(9): 2681-2696.
- Lin, S., Yu, Y., Zhang, Z., et al. The synergistic mechanisms of citric acid and oxalic acid on the rapid dissolution of kaolinite. Applied Clay Science, 2020, 196: 105756.
- Lin, S., Yu, Y., Zhong, M., et al. The dissolution behavior of feldspar minerals in various low-molecular-weight organic acids. Materials, 2023, 16(20), 6704.
- Liu, S., Chen, A., Shen, Z., et al. Fluid-rock interaction and dissolution of feldspar in the Upper Triassic Xujiahe tight sandstone, western Sichuan Basin, China. Open Geosciences, 2018, 10(1): 234-249.
- Ma, B., Cao, Y., Jia, Y., et al. Feldspar dissolution with implications for reservoir quality in tight gas sandstones: Evidence from the Eocene Es4 interval, Dongying Depression, Bohai Bay Basin, China. Journal of Petroleum Science and Engineering, 2017, 150: 74-84.
- Maher, K. The dependence of chemical weathering rates on fluid residence time. Earth and Planetary Science Letters, 2010, 294(1-2): 101-110.
- Manley, E. P., Evans, L. J. Dissolution of feldspars by low-molecular-weight aliphatic and aromatic acids. Soil Science, 1986, 141(2): 106-112.
- Marsala, A., Wagner, T. Mass transfer and fluid evolution in late-metamorphic veins, Rhenish Massif (Germany): Insight from alteration geochemistry and fluid-mineral equilibria modeling. Mineralogy and Petrology, 2016, 110: 515-545.
- Meng, X., Zhou, Y., Chen, Y., et al. Differential sedimentary response of coal seams in coal-bearing rock series and oil and gas exploration: A case study of the j1b formation in the mahu slope area. Acta Sedimentologica Sinica, 2023, 41(4): 1212-1226. (in Chinese)
- Ming, D., Chang, X., Shang, F., et al. Heterogeneity of pore structure in braided river delta tight sandstone reservoirs: Implications for tight oil enrichment in the Jurassic Badaowan Formation, Central Junggar Basin. Natural

- Resources Research, 2025, 34: 1743-1771.
- Morrey, J. R., Krupka, K. M., Dove, F. H. MINTEQ2 geochemical code: Provisionary organic data base (p. 61). 1985. Pacific Northwest Labs.
- Palandri, J. L., Kharaka, Y. K. A compilation of parameters of water-mineral interaction kinetics for application to geochemical modeling. Menlo Park, U.S. Geological Survey, 2004.
- Schleicher, A. M., Tourscher, S. N., van der Pluijm, B. A., et al. Constraints on mineralization, fluid-rock interaction, and mass transfer during faulting at 2-3 km depth from the SAFOD drill hole. Journal of Geophysical Research: Solid Earth, 2009, 114(B4): B04202.
- Shan, X., Guo, H., Chen, X., et al. Genesis of densification of low-permeability tight sandstone reservoirs: A case study of Lower Jurassic Badaowan Formation in Mobei-Mosuowan Swell, Junggar Basin. Acta Sedimentologica Sinica, 2021, 40(5): 1406-1418. (in Chinese)
- Shi, X., Qi, X., Shi, Q., et al. Characteristics of Jurassic source rocks and oil sources of Sikeshu Depression in the Junggar Basin. Chinese Journal of Geology (Scientia Geologica Sinica), 2020, 55(4): 974-988. (in Chinese)
- Sonnenthal, E., Spyoher, N. Drift-scale coupled processes (DST and THC seepage) models. Office of Scientific & Technical Information Technical Reports, 2001.
- Sorai, M., Ohsumi, T., Ishikawa, M. Nanoscale surface observation of feldspar dissolved under supercritical CO₂-water-mineral system. Energy, 2005, 30(11-12): 2334-2343.
- Steefel, C. I., Lasaga, A. C. A coupled model for transport of multiple chemical species and kinetic precipitation/dissolution reactions with application to reactive flow in single phase hydrothermal systems. American Journal of Science, 1994, 294(5): 529-592.
- Steefel, C. I., Maher, K. Fluid-rock interaction: A reactive transport approach. Reviews in Mineralogy and Geochemistry, 2009, 70(1): 485-532.
- Sun, J., Xue, J., Zeng, D., et al. Deep tight reservoir characteristics and main controlling factors of Badaowan formation in the central Junggar basin. Journal of Northeast Petroleum University, 2017, 41(1): 1-10+135. (in Chinese)
- Surdam, R. C., Boese, S. W., Crossey, L. J. The chemistry of secondary porosity, in Clastic Diagenesis, edited by David A. McDonald and Ronald C. Surdam, American Association of Petroleum Geologists, Tulsa, pp. 127-149, 1984.
- Surdam, R. C., MacGowan, D. B. Oilfield waters and sandstone diagenesis. Applied Geochemistry, 1987, 2(5-6): 613-619.
- Thomas, F., Masion, A., Bottero, J. Y., et al. Aluminum (III) speciation with acetate and oxalate. A potentiometric and aluminum-27 NMR study. Environmental Science & Technology, 1991, 25(9): 1553-1559.
- Thyne G. A model for diagenetic mass transfer between adjacent sandstone and shale. Marine and Petroleum Geology, 2001, 18(6): 743-755.
- Welch, S. A., Ullman, W. J. The effect of organic acids on pla-

- gioclase dissolution rates and stoichiometry. Geochimica et Cosmochimica Acta, 1993, 57(12): 2725-2736.
- Welch, S. A., Ullman, W. J. Feldspar dissolution in acidic and organic solutions: Compositional and pH dependence of dissolution rate. Geochimica et Cosmochimica Acta, 1996, 60(16): 2939-2948.
- Xi, K., Cao, Y., Zhu R., et al. Integration of diagenesis, porosity evolution, and oil emplacement in lacustrine tight sandstone reservoirs: A review with illustrative cases from the major oil-bearing basins in China. AAPG Bulletin, 2024, 108(4): 691-718.
- Yang, L., Steefel, C. I. Kaolinite dissolution and precipitation kinetics at 22 °C and pH 4. Geochimica et Cosmochimica Acta, 2008, 72(1): 99-116.
- Yang, Y., Min, Y., Jun, Y. Effects of Al/Si ordering on feldspar dissolution: Part II. The pH dependence of plagioclase' dissolution rates. Geochimica et Cosmochimica Acta, 2014, 126: 595-613.
- Yu, J., Zhang, X., Qi, L., et al. Densification mechanism of coal-bearing glutenite reservoirs: An example from Badaowan Formation in AH5 well area, Junggar Basin. Journal of China University of Mining & Technology, 2023, 52(6): 1216-1230.
- Yuan, G., Cao, Y., Yang, T., et al. Porosity enhancement potential through mineral dissolution by organic acids in the diagenetic process of clastic reservoir, Earth Science Frontiers, 2013, 20(5): 207-219.
- Yuan, G., Cao, Y., Gluyas, J., et al. Reactive transport modeling of coupled feldspar dissolution and secondary mineral precipitation and its implication for diagenetic interaction in sandstones. Geochimica et Cosmochimica Acta, 2017, 207: 232-255.
- Yuan, G., Cao, Y., Gluyas, J., et al. Feldspar dissolution, authigenic clays, and quartz cements in open and closed sandstone geochemical systems during diagenesis: Typical examples from two sags in Bohai Bay Basin, East China. AAPG Bulletin, 2015, 99(11): 2121-2154.
- Yuan, G., Cao, Y., Schulz, H. M., et al. A review of feldspar alteration and its geological significance in sedimentary

- basins: From shallow aquifers to deep hydrocarbon reservoirs. Earth-science reviews, 2019, 191: 114-140.
- Zeng, L, Jin, J., Ma, W., et al. Petroleum generation kinetics of Jurassic coals in the southern margin of the Junggar Basin. Geochimica, 2021, 50(3): 282-293. (in Chinese)
- Zhang, A., Chen, S., Tang, D., et al. The study on diagenetic characteristics of coal measures sandstone reservoir in Xishanyao formation, southern margin of the Junggar basin. Energies, 2022, 15(15): 5499.
- Zhang, L., Lüttge A. Theoretical approach to evaluating plagioclase dissolution mechanisms. Geochimica et Cosmochimica Acta, 2009, 73(10): 2832-2849.
- Zhang, Y., Jiang, S., Li, F. Influence of sandstone-shale contacts on feldspar diagenesis in the sandstone reservoir of the Shahejie Formation in the Dongying depression, Bohai Bay basin. Acta Geologica Sinica, 2021, 95(3): 883-894. (in Chinese)
- Zhang, Y., Zeng, J., Yu, B. Experimental study on interaction between simulated sandstone and acidic fluid. Petroleum Science, 2009, 6: 8-16.
- Zhu, C., Lu, P. Alkali feldspar dissolution and secondary mineral precipitation in batch systems: 3. Saturation states of product minerals and reaction paths. Geochimica et Cosmochimica Acta, 2009, 73(11): 3171-3200.
- Zhu, C., Lu, P., Zheng, Z., et al. Coupled alkali feldspar dissolution and secondary mineral precipitation in batch systems: 4. Numerical modeling of kinetic reaction paths. Geochimica et Cosmochimica Acta, 2010, 74(14): 3963-3983.
- Zhu, Y., Vieth-Hillebrand, A., Noah, M., et al. Molecular characterization of extracted dissolved organic matter from New Zealand coals identified by ultrahigh resolution mass spectrometry. International Journal of Coal Geology, 2019, 203: 74-86.
- Zhu, Y., Vieth-Hillebrand, A., Wilke, F. D., et al. Characterization of water-soluble organic compounds released from black shales and coals. International Journal of Coal Geology, 2015, 150: 265-275.